Enhanced Photocatalytic Water Splitting with Two-Dimensional van der Waals Heterostructures of BAs/WSeTe

Hanifa BiBi[1], Abdul Jalil[1], Syed Zafar Illyas,[1] Azeem Ghulam Nabi,[2,3,*] and Devis Di Tommaso[3,4,*]

AFFILIATIONS

[1] Department of Physics, Allama Iqbal Open University, Islamabad, 44000, Pakistan

[2] Department of Physics, Hafiz Hayat Campus, University of Gujrat, Gujrat, 50700, Pakistan

[3] Department of Chemistry, School of Physical and Chemical Sciences, Mile End Road, London, Queen Mary University of London, E1 4NS, U.K.

[4] Digital Environment Research Institute, Queen Mary University of London, Empire House, 67-75 New Road, London E1 1HH, UK

ABSTRACT

The photocatalytic efficiency of monolayer materials can be significantly enhanced by constructing two-dimensional van der Waals heterostructures. This study presents first principles calculations based on density functional theory to investigate the electronic properties and photocatalytic mechanism of van der Walls heterostructures of boron arsenide (BAs) with the Janus MXY (M=W; X/Y=Se, Te) monolayers, with and without Se vacancies. Results from binding energies, phonon spectra, and *ab initio* molecular dynamics simulations indicate that the heterostructures are stable from all respects. Moreover, all the heterostructures exhibit direct bandgaps with valence band maxima and conduction band minima suitable for water splitting. Additionally, these heterostructures possess high optical absorption coefficients in the visible and ultraviolet regions. In particular, our calculations predict BAs/WTeSe, with and without Se vacancies, as promising candidates for photocatalytic water splitting applications.

Keywords

First principles calculations; 2D materials; Heterostructure; Electric field; Water splitting.

INTRODUCTION

The finite nature of fossil fuels, coupled with their detrimental environmental impact and contribution to climate change, has exacerbated environmental contamination and energy crises, posing significant challenges to humanity [1]. Finding a sustainable energy source to replace finite fossil fuels is crucial. Hydrogen generated by photocatalytic water splitting is regarded as a sustainable, clean, and renewable energy source for the future [2][3][4]. However, finding the right photocatalyst is essential to producing hydrogen energy from water splitting. The large band gap and improper alignment of band edge position is the main hurdle for a suitable photocatalyst for water splitting [5], [6][7].

Graphene, a two-dimensional (2D) material, has been extensively studied for its applications in electronic and optoelectronic devices, even it lacks a tunable band gap [8]. Consequently, new types of 2D materials has been extensively explored in recent years, including phosphorene [9], analogues transition metal dichalcogenides (TMDs) [10], and MXenes [11]. Compared with the bulk counterparts, TMDs have enhanced charge transfer and separation capabilities due to their large specific surface area, promising optoelectronic, transistors and sensors devices[10]. Among TMDs, WX_2 (X = S, Se, Te) [12] monolayers have been widely studied theoretically and experimentally. The WS_2, WSe_2 and $MoSe_2$ monolayers are excellent high-temperature thermoelectric materials. A recent breakthrough in the realm 2D TMDs has led to the synthesis of Janus MXY (M=W, Mo; X/Y=Se, S, Te) through vulcanization or selenidation experiments employing the CVD method [13] Unlike their mirror-symmetrical counterparts MoS_2 and $MoSe_2$, the MoSSe monolayer is fabricated via selective selenization of the top atomic layer in a single-layer MoS2 structure. The electronegativity difference between sulfur and selenium atoms induces interlayer polarization in Janus materials, enabling coupling with the inherent interlayer built-in polarization field. This unique property introduces an additional degree of freedom for modulating their physicochemical properties, garnering significant attention due to their novel features and promising applications. Moreover, Janus-WSeTe or Janus-WTeSe monolayers are direct band gap semiconductors with moderate band gaps [14]. Unfortunately, not all 2D materials are good for water splitting because their band gap value is large, and the band edge alignment is located far from the redox potentials.

To address these limitations, van der Waals heterostructures (vdWHs) have been proposed as a promising strategy to engineer suitable band edge positions for water splitting splitting [15]–[21]. Arsenide semiconductors, such as boron arsenide (BAs)[22], aluminum arsenide (AlAs) [23], gallium arsenide (GaAs) [5], [24], and indium arsenide (InAs) [25], have emerged as promising candidates for vdWHs due to their favorable band alignments and light absorption properties. These materials belong to Group III-V family of compound semiconductor materials [26]–[29] and play an vital role

to make microwave devices [30][31], Hall devices [32], high-speed digital circuits [33], lasers [34][35], magneto-resistive devices [7] [35], and detectors [36]. Hexagonal BAs monolayer with a flat honeycomb structure like graphene has drawn attention as potential photocatalyst for water splitting [37]. BAs has a direct band gap, high carrier mobility, high in-plane mechanical stability and it is only semiconductor material with an ultrahigh thermal conductivity of 2000 W/m·K at room temperature. Consequently, BAs monolayer has been recently combined with many other 2D materials such as the vdWHs BAs/$MoTe_2$[6], BAs/$MoSe_2$[38], BAs/SnC[39], and BAs/GaN[40].

This paper investigates the photocatalytic properties of BAs/Janus WSeTe and BAs/Janus WTeSe vdWHs using density functional theory (DFT) calculations as a possible direct Z-scheme photocatalyst. The stacking-based approaches have been employed to investigate the electrical, optical and photocatalytic properties absorption of all the suggested systems. We found that many configurations of these heterostructure are suitable to tune optoelectronic characteristics for photo-catalysis applications, either type-II or Z-scheme. Although the built-in electric field under various stacking configurations favours the development of Z-scheme charge transfer, not all of them belong to Z-scheme, according to work function and charge density difference. In actuality, the classification of the system as type II or Z-scheme depends on the competition between charge separation and interlayer e-h recombination. Furthermore, by introducing Se vacancy defects, which successfully flip the charge transfer channel in Janus BAs/WSeTe heterostructures from type II to Z-scheme, this competitive relationship may be effectively regulated. Perhaps, most remarkably, Se vacancy defects lengthen the interval of time between electron (hole) transmission. Our findings show that the BAs/Janus WSeTe vdWHs have strong photocatalytic activity and that the proposed configuration-II is ideally suited for highly efficient water splitting.

METHODS

All DFT calculations were conducted using the Vienna ab initio simulation package (VASP) [41] and the projector augmented wave (PAW) potential method [42]. Geometry optimization and *ab initio* molecular dynamics (AIMD) were performed using the Perdew–Burke–Ernzerhof (PBE) generalized gradient approximation (GGA) [43] in conjunction with Grimme's D3 functional (PBE-D3) to accurately describe the van der Waals interactions between BAs and Janus-WSeTe [44]. As generally PBE underestimates the band gap of semiconductors, single point calculations were conducted at the hybrid DFT level with the HSE06 (Heyd–Scuseria–Ernzerhof) and the same functional was used to compute the optical properties of above mentioned heterostructures and monolayers [45]. Convergence tolerances were set to 10^{-6} eV for the energy and 0.01 eV $Å^{-1}$ for the force. To ensure

calculation accuracy, the *k*-point (Monkhorst–Pack) grid was set to (15×15×1) together with a cutoff energy of 520 eV for ensuring calculation accuracy. The vacuum space was to 25 Å to minimise the interaction between adjacent layers. Ab initio molecular dynamics (AIMD) simulations was performed with a (4×4×1) supercell at the *Γ* point for 5 ps using a 1 fs timestep in the an NVT (300 K) ensemble [46]. The phonon dispersion curves calculations were also performed with a 4 × 4 × 1 supercell in the framework of the frozen-phonon approximation [48].

RESULTS AND DISCUSSION

Structural properties. To construct the initial models of 2D BAs-Janus WSeTe vdWHs, the structures of the isolated hexagonal BAs and WSeTe monolayers were optimized first. The optimized structural parameters of BAs and WSeTe are summarized in **Table 1**. The lattice constants of BAs are $a = b = 3.32$ Å with bond length of B-As is 1.96 Å. The lattice constants of BAs are $a = b = 3.32$ Å, and the B-As bond length is 1.96 Å. The Janus WSeTe monolayer has lattice constants of $a = b =$ 3.45 Å, with bond length 2.55 Å and 2.71 Å between W-Se and W-Te atoms, respectively. The calculated values of lattice parameters and bond lengths of both structures are consistent with those in previous studies [6], [49], [50]. The BAs with Janus-WSeTe and BAs with Janus-WTeSe monolayers were used to construct 12 vdW heterostructures configurations. They are categorized into two different classes: (i) BAs/Janus WSeTe vdWHs, where the BAs monolayer is close to Se atom of the Janus-WSeTe monolayer; (ii) BAs/Janus WTeSe vdWHs, where the BAs layer is close to Te atoms of the Janus WTeSe monolayer. For these two classes of heterostructures, six different stacking configurations are possible, as shown in **Figure 1**.

Table 1. Structural and energetic parameters of the isolated hexagonal BAs and WSeTe monolayers and of the 2D BAs-Janus WSeTe vdWs heterostructures: lattice parameter *a* (Å); Band gap (E_g), formation energy △E (eV); distance *d* (Å) between BAs and Janus-WSeTe monolayers in the six heterostructure configurations.

System	**a (Å)**	**d (Å)**		**E_g (eV)**		**△E**
Method		**PBE**	**PBE-D3**	**HSE**	**PBE**	
BAs						
	3.328	–	–	1.370	0.753	–
WSeTe						
	3.451	–	–	1.807	1.353	–
BAs/Janus WSeTe						
Stacking-A	3.392	4.208	3.710	1.294	0.712	-0.198
Stacking-B	3.392	4.214	3.520	1.431	0.796	-0.225
Stacking-C	3.391	4.214	3.610	1.300	0.745	-0.208
Stacking-D	3.392	4.216	3.440	1.189	0.682	**-0.252**
Stacking-E	3.390	4.208	3.780	1.279	0.694	-0.189
Stacking-F	3.391	4.172	3.390	1.285	0.709	-0.251
BAs/ Janus WTeSe						

Stacking-A	3.390	4.470	3.990	0.861	0.374	-0.195
Stacking-B	3.390	4.259	3.780	0.888	0.382	-0.223
Stacking-C	3.391	4.448	3.851	0.817	0.309	-0.203
Stacking-D	3.391	4.128	3.610	0.663	0.192	-0.254
Stacking-E	3.391	4.462	4.030	0.924	0.466	-0.186
Stacking-F	3.389	4.117	3.560	0.931	0.530	**-0.264**
BAs/ Janus WTeSe (Vacancy)						
	3.375	----	3.513	0.510	0.068	----

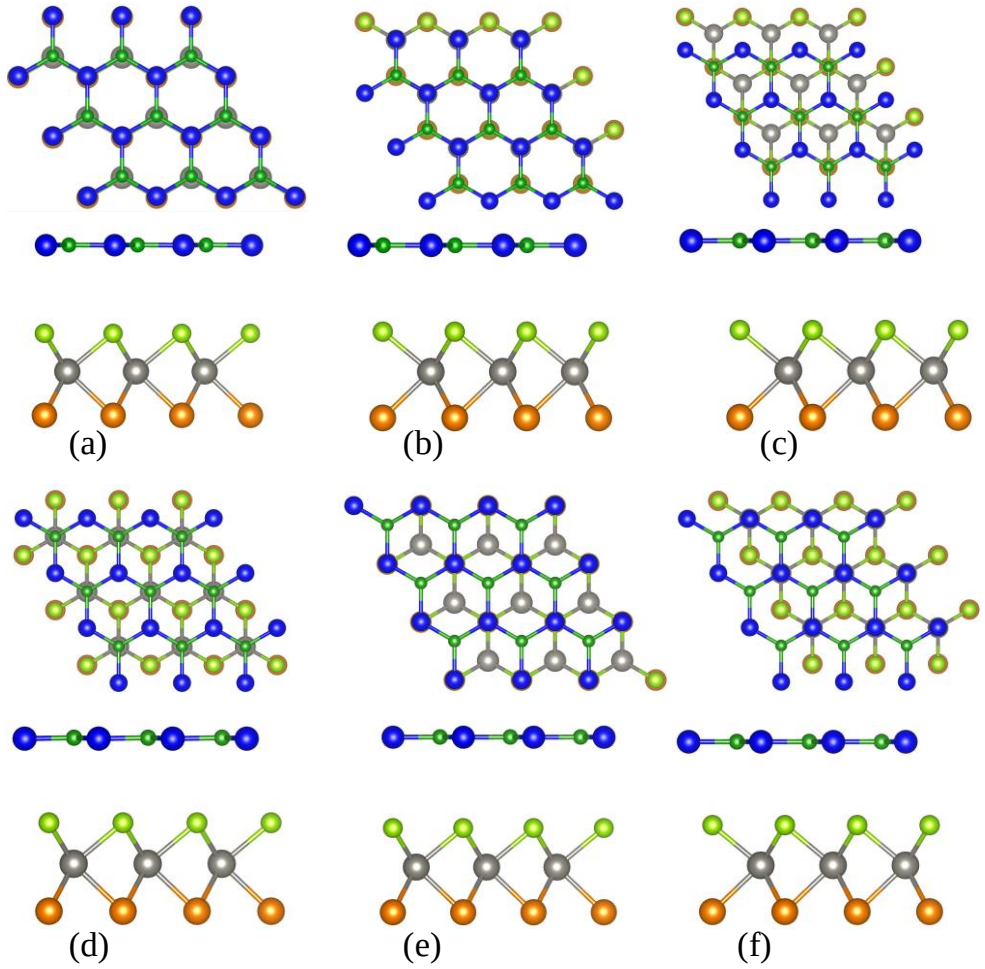

Figure 1: Top and side views of different configurations of vdWHs obtained from the stacking of BAs and Janus-WSeTe: **(a)** stacking-A, the B and As atom sits on the top of W and Se atom, respectively; **(b)** stacking-B, the B and As atom sits on the top of Se and W atom, respectively; **(c)** stacking-A, the As atom is on the hollow site of the hexagonal, the B atom occupies the top of Se atom); **(d)** stacking-D, the As atom is on the hollow site of the hexagonal, the B atom occupies the top of W atom, respectively; **(e)** stacking-E, the As atom sits on the top of Se atom, while the B atom is on the center of the hexagonal site; **(f)** stacking-F, the As atom sits on the top of W atom, while the B atom is on the center of the hexagonal site, BAs/Janus WSeTe vdW heterostructure. The BAs/Janus WTeSe vdWHs are formed by swapping the positions of Se and Te atoms in the six configurations **(a-f)**.

The computed values of lattice parameters and interlayer distances of the optimized BAs/WSeTe vdWHS are listed in **Table 1**. Moreover, their formation energies (ΔE) were evaluated according to:

$$\Delta E = E_{\text{heter}} - E_{\text{layer1}} - E_{\text{layer2}} \quad (1)$$

where E_{heter}, E_{layer1}, and E_{layer2} are the total energies of the heterostructure, BAs, and Janus WSeTe monolayer, respectively. The two most stable heterostructures according to the values of formation energy are BAs/Janus WSeTe (stacking-D) in **Figure 1(d)** and BAs/Janus WTeSe (stacking-F) vdWHs in **Figure 1(f)**. The total energy of these structures is smaller than other structures by at least 10 meV. The following structures were considered to investigate the vibrational, electronic, photocatalytic (water splitting), and optical properties: (i) BAs/Janus WSeTe (H-I); (ii) BAs/Janus WTeSe (H-II) and (iii) BAs/Janus WTeSe with Se vacancies (H-III). The phonon dispersions of BAs, WSeTe, and the H-I, H-II heterostructures in **Figure 2** confirm their structural stability, because no imaginary frequencies are found in these phonon spectra. Furthermore, the H-III heterostructure exhibits dynamic stability, as corroborated by its phonon spectra presented in **Figure S2** (Supporting Information). Moreover, AIMD simulations without dispersion correction show these heterostructures are thermodynamically unstable due the increase in interlayer spacing between BAs and WSeTe or BAs and WTeSe monolayers separating apart. Furthermore, the obtained lattice parameters of the monolayer, WSeTe, BAs and heterostructures H-I, H-II and H-III are 3.45 Å, 3.33 Å and 3.39 Å, 3.38 Å and 3.37, respectively, in agreement with the previous studies [37]. Due to higher value of lattice mismatch, many defects are invariably created at the interface when two single-crystalline materials are formed or fused together. For BAs and Janus-WSeTe, the lattice mismatch is 3.3%, which is in limit to avoid surface defects [51][52]. Finally, in **Table 1** the includion of dispersion correction in the PBE functional has a significant influence on the stability of heterostructures [53]. The most stable heterostructures H-I (stacking-D) and H-II (stacking-F) have lower interlayer spacing, d = 3.44 Å and d = 3.56 Å, respectively, and these heterostructures are thermodynamically stable.

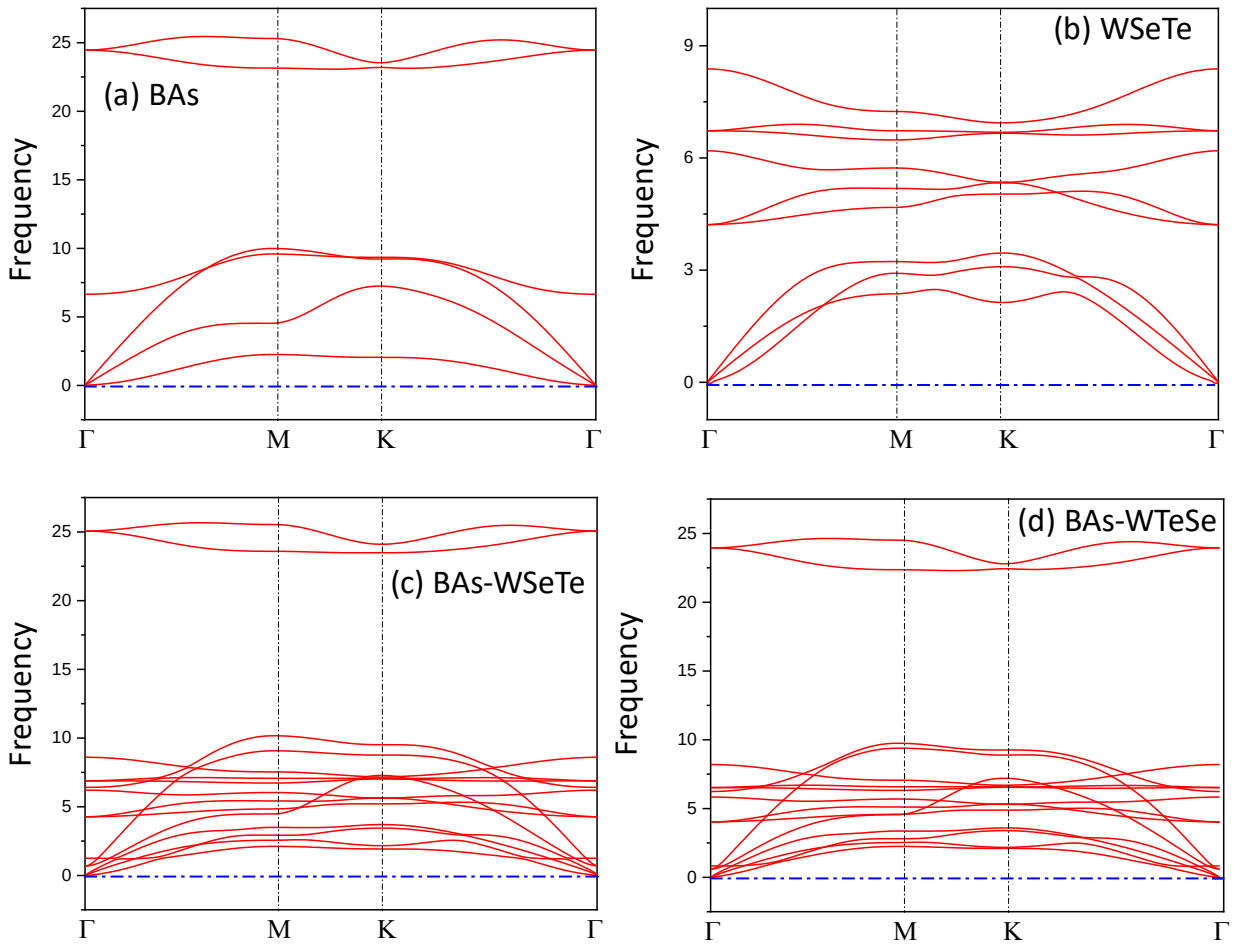

Figure 2. The phonon spectra of **(a)** H-I, **(b)** H-II, and **(c)** H-III heterostructures.

Electronic properties. The band structure provides insights into the electronic properties of a material. First, the electronic properties of the BAs and Janus MoSeTe monolayers are considered before exploring those of the BAs/Janus WSeTe heterostructure. The band structures of Janus WSeTe and BAs, computed at the PBE and HSE06 levels of theory, are presented in **Figure 3**. The band gap values for Janus WSeTe and BAs monolayers, calculated using the HSE06 hybrid functional, are 1.36 and 1.8 eV, respectively. Moreover, both Janus-WSeTe and BAs are direct band gap semiconductor, because in each case the conduction band minima (CBM) and the valence band maxima (VBM) lies on the same high-symmetric K point of the Brillouin zone. Most importantly, the direct band gap semiconductor nature of these monolayers remains preserved after the formation of heterostructures.

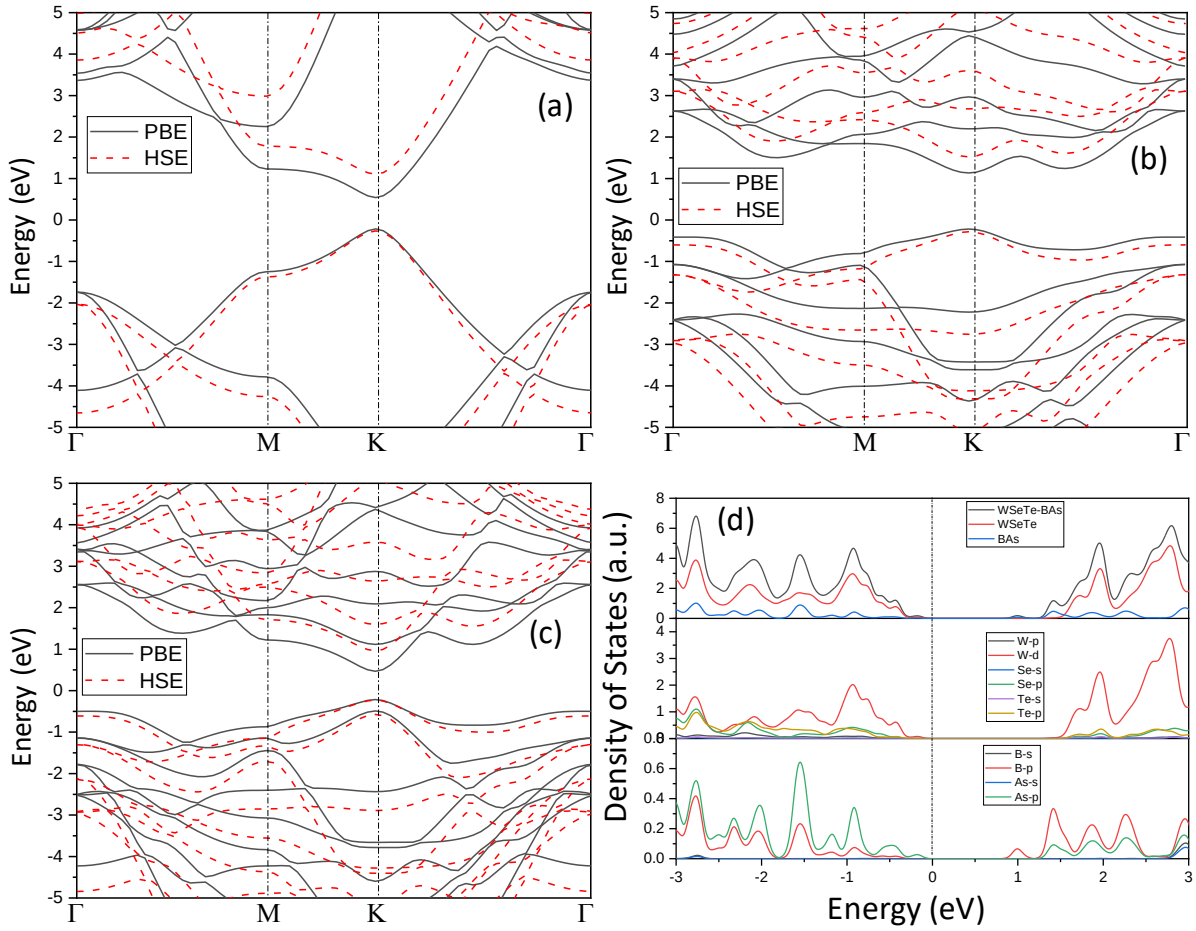

Figure 3. The band structures **(a)** BAs, **(b)** Janus WTeSe, **(c)** H-I heterostructure computed using the PBE (black solid lines) and HSE (red dashed lines) functionals. **(d)** Density of states of the H-I heterostructure.

To investigate the electronic properties of H-I, H-II and H-III heterostructures in more detail the total density of states (TDOS) and partial density of states (PDOS) are calculated for these heterostructure. The CBM and VBM of the MoTeSe monolayer are formed by the Te-5p, Se-4p and W-4d states, respectively[50]. Furthermore, VBM of the BAs monolayer is composed of the As-4p states, and the CBM is consisted of B-2p states. These results are in agreement with the other studies [22]. As a result, the unique type-II and Z-scheme band alignments are naturally formed at the interface, which provides favorable conditions for the application of heterostructure in photocatalytic water splitting. **Figure 4** show the projected band structure of H-I and H-II. It is clear that for each heterostructure VBM is composed of of WSeTe or WTeSe (blue color) while CBM is consisted of BAs (red color). The H-I show smaller interlayer band gap (0.66 eV) than H-II (1.18 eV) as shown in **Figure 4**. When Se vacancies were created in H-II, the interplanar band gap (**Figure S1** in Supporting Information) was further reduced (0.51 eV).

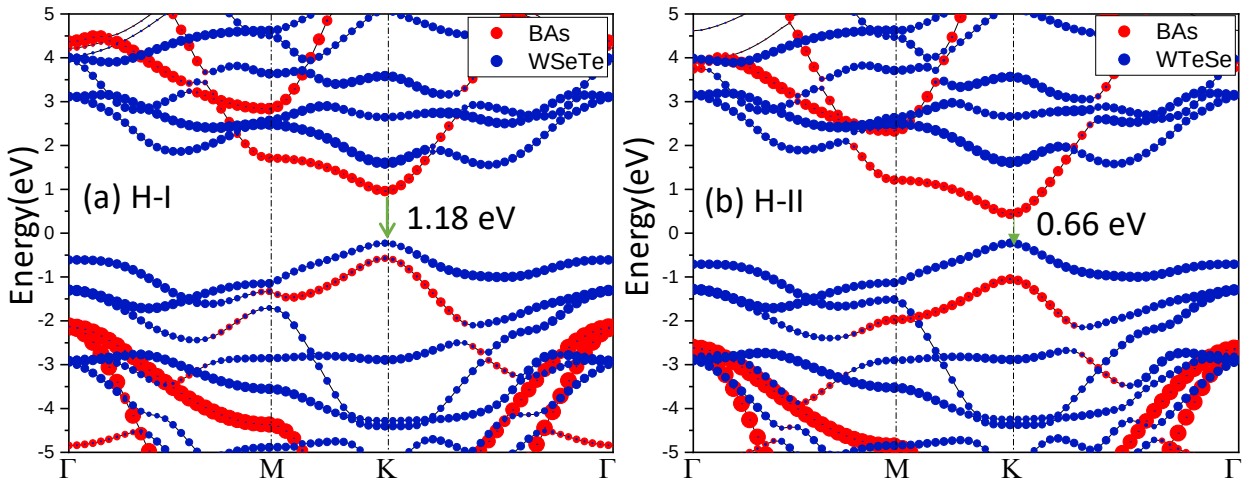

Figure 4. Projected band structures of the **(a)** H-I and **(b)** H-II heterostructures.

Photocatalytic water splitting characteristics. The design of direct Z-scheme photocatalysts either experimentally or theoretically remains a challenge [54]. DFT calculations can be used to determine the type of the heterostructure whether it is direct Z-scheme or type II configuration [55]. To understand this mechanism, the charge density difference ($\Delta\rho$), the build-in electric field (E_{int}), the electron hole recombination, the effective masses, and the interlayer band gaps are important parameters to be investigated in detail. The $\Delta\rho$ on the interface was computed according to:

$$\Delta\rho = \rho_{BAs/WSeTe} - \rho_{BAs} - \rho_{WSeTe} \quad (2)$$

where $\rho_{BAs/WSeTe}$, ρ_{BAs}, and ρ_{WSeTe} represent the charge density of the BAs/WSeTe or BAs/WTeSe vdWHTs, Bas, and WSeTe monolayers, respectively. The $\Delta\rho$ plots are given in the insets of **Figure 5.** When two monolayers are in contact, electrons will flow through the interface due to the difference in their Fermi levels. Until the Fermi levels reach to equilibrium, the charge will keeping on moving across the interface. The Fermi level can be found if the value of work function is known by using the flowing relation:

$$\phi = E_{vac} - E_F \quad (3)$$

where E_{vac} and E_{F} are the vacuum and Fermi levels, respectively. The value of work function for BAs is 5.23 eV and WSeTe is 5.37 eV. Since the BAs monolayer has low Fermi level, the charge is transferred from the Janus-WSeTe or Janus-WTeSe to the BAs monolayer. The electrons will accumulate on BAs surface while holes gather on Janus-WSeTe or Janus-WTeSe surface. The built-in electric field (E_{int}), from WSeTe to BAs, will be formed when charge accumulates at the interface. This electric field will stop the further flow of charges, when the Fermi levels of both BAs and Janus-WSeTe or Janus-WTeSe monolayers reaches equilibrium, resulting in the formation of heterostructure (H-I, H-II and H-III). However, Janus-WSeTe or Janus-WTeSe are polar systems with

an opposite intrinsic electric field, which offsets the E_{int} and lead to a net effective electric field E_{eff} across the heterostructure. The value of E_{eff} depends on electrostatic potential ($\Delta\phi$) and is given as

$$E_{eff} = \frac{\Delta\phi}{ed} \tag{4}$$

where *d* is the thickness. The values of electrostatic potential ($\Delta\phi$), given in equation 4, for H-I, H-II and H-III heterostructures are 0.39, 0.63 and 0.64 eV, respectively [12], [56]. This E_{eff} produced in the heterostructure could effectively inhibit the recombination of photo-generated e^-/h^+ pairs and enhance carrier separation in H-I, H-II and H-III heterostructures, as shown in **Figure 5(g)**.

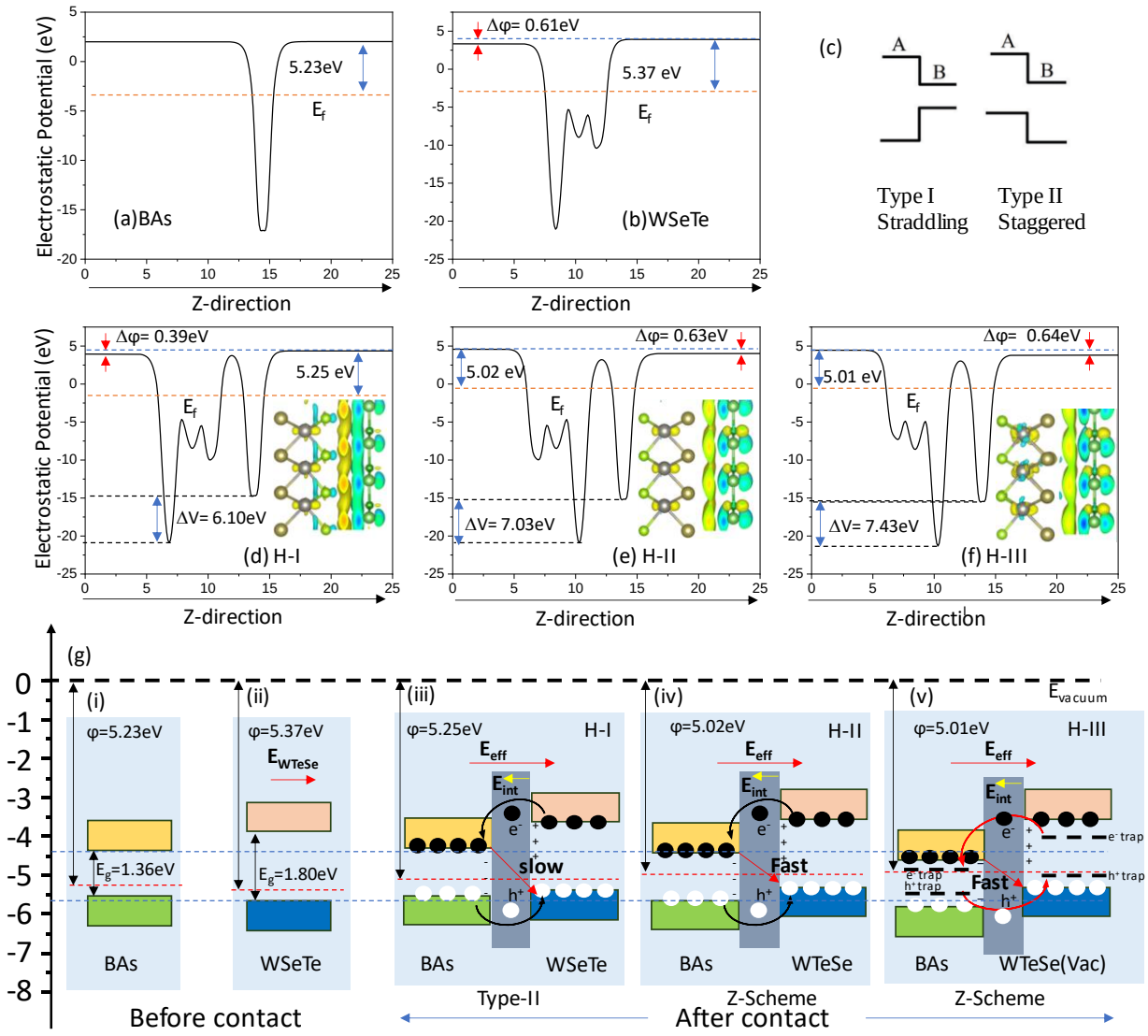

Figure 5. Electrostatic potential of **(a)** BAs; **(b)** WSeTe; **(d)** H-I, I H-II; **(f)** H-III. **(h)** Type-I and Type-II heterostructures mechanism. **(g)** The schematic diagram of Z-scheme mechanism for photocatalysis of heterostructure.

The E_{eff} value of H-II is considerably higher than that of H-I. This indicates a faster electron-hole (e-h) recombination rate in the H-I heterostructure and a slower rate in the H-II heterostructure. Consequently, the H-II heterostructure exhibits superior catalytic performance and aligns with the Z-

scheme photocatalytic mechanism [14][26]. In Z-scheme photocatalysts, the interlayer e-h recombination should be much higher than intralayer band gap to work it without any mediators. This is only possible if the heterostructures have much smaller interlayer band gap than intralayers and a larger ratio of effective masses ($D = m^*_h/m^*_e$) indicates that e-h recombination will be supressed to enhance the catalytic performance (**Table S1** in Supporting Information). The above results show that H-I is type-II while H-II heterostructure is a direct Z-scheme photocatalyst.

For effective water decomposition catalysis, the band edges of the photocatalyst must straddle the water redox potentials. Moreover, water splitting can only occur on the surface of heterostructures if the conduction band minimum (CBM) of semiconductor-II is more positive than the reduction potential of H^+/H_2, and the valence band minimum (VBM) is more negative than the oxidation potential of O_2/H_2O. Therefore, we further investigated the band alignments of H-I, H-II, and H-III, with the results presented in **Figure 5**. The BAs and WTeSe monolayers are presented for comparison. The reduction potential of H^+/H_2 and oxidation potential of O_2/H_2O at different pH values is given by

$$E^{\mathrm{red}}_{\mathrm{H^+/H_2}} = -4.44\mathrm{eV} + \mathrm{pH} \times 0.059\mathrm{eV} \quad (5)$$

$$E^{\mathrm{oxd}}_{\mathrm{O_2/H_2O}} = -5.67\mathrm{eV} + \mathrm{pH} \times 0.059\mathrm{eV} \quad (6)$$

At a pH of 7, the reduction and oxidation potentials are -4.03 eV and -5.26 eV, respectively. It is evident from **Figure 5** that the CBM energies of BAs, WSeTe monolayers, and H-I and H-II heterostructures lie higher than the reduction potential of H_+/H_2, while their VBM energies are lower than the oxidation potential of O_2/H_2O. This alignment of band positions is favorable for photocatalytic water splitting. Figure 5 also illustrates the photocatalytic reaction mechanism and the alteration of photoexcited carriers for H-I, H-II, and H-III heterostructures. Upon interaction with light, the heterostructure absorbs energy, causing electrons in the VBM to transition to the CBM, generating holes in the VBM and electrons in the CBM. Subsequently, the photoinjected electrons in the CBM of BAs transfer to the VBM of Janus WSeTe, as shown in **Figure 5g(iii)**. However, in this configuration, the interlayer band gap of 1.18 eV leads to a rapid electron-hole recombination process due to the small value of $\Delta\phi$ = 0.39 eV. Replacing the Se atom with a Te atom in the H-II heterostructure significantly reduces the interlayer band gap to 0.66 eV. This reduction in interlayer band gap slows down the e-hrecombination rate, facilitating charge accumulation at the VBM and CBM due to the higher value of $\Delta\phi$ = 0.63 eV. This, in turn, enhances the catalytic efficiency of the heterostructure. Furthermore, introducing Se vacancies in the H-III heterostructure further decreases the band gap to 0.52 eV. These vacancies generate electron and hole trapping states at the VBM and CBM, which effectively increase the mass of electrons and holes and suppress electron-hole

recombination at the interlayer. Similar to the previous case, this further decreases the rate of electron-hole recombination, potentially influencing the catalytic performance.

Optical properties. The photocatalytic efficiency of a photocatalyst depends on its ability to capture photons in visible region (380 to 760 nm). The light absorption coefficient is given as:

$$\alpha = \frac{\sqrt{2}\omega}{c}\left\{[\varepsilon_1^2(\omega) + \varepsilon_2^2(\omega)]^{1/2} - \varepsilon_1(\omega)\right\}^{1/2} \quad (7)$$

where c and ω show the and the speed of light angular frequency in vacuum, the dielectric constant has real $\varepsilon_1(\omega)$ and imaginary $\varepsilon_2(\omega)$ parts. **Figure 5** demonstrates the light absorption coefficients of Janus-WSeTe, BAs, H-I and H-II heterostructures. The maximum light absorption coefficients in visible region of light of BAs around 150, 210, 280 and 370 nm (ultraviolet region) and 470 and 550 nm (visible region)[12]. WSeTe monolayer has peaks at 322 nm and 610nm. The absorption peaks for the WSeTe monolayer shows a wide absorption range in the visible and ultraviolet regions is better than that of BAs.

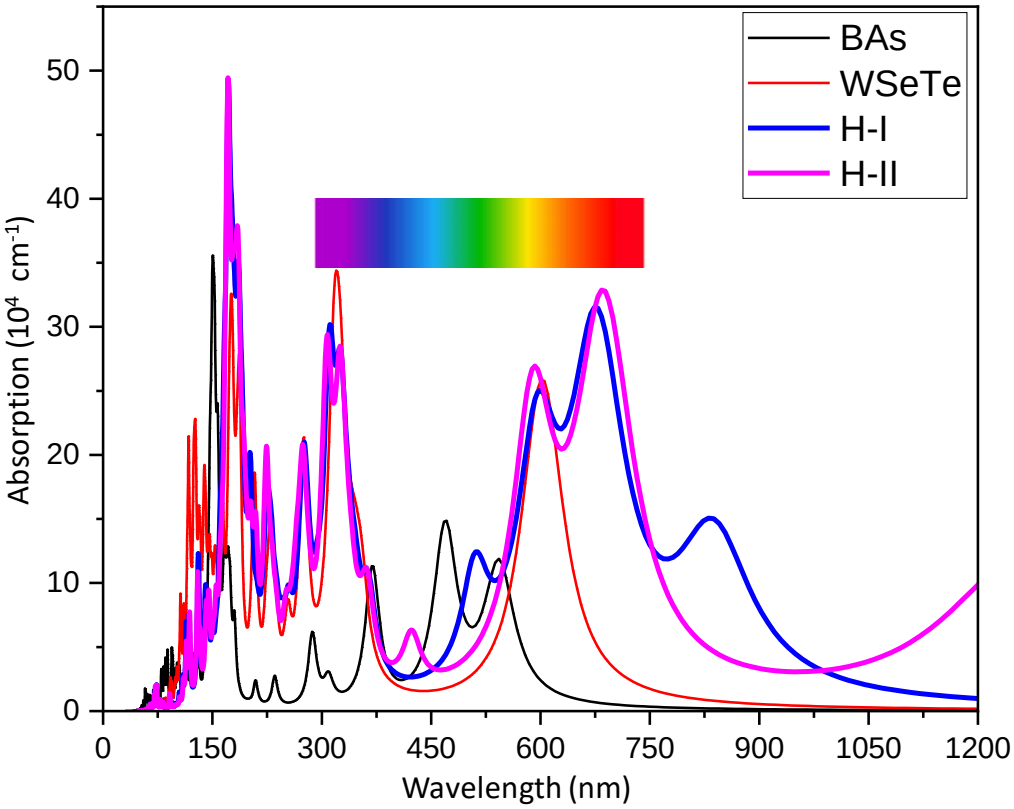

Figure 6. The absorption coefficient of the monolayers BAs, WSeTe, and two different heterostructures.

Compared to monolayers, the heterostructures introduce two new peaks in the visible region: 424 nm for H-I (blueshift) and 514 nm for H-II (redshift). This not only significantly expands the light absorption range but also substantially increases the absorption intensity, demonstrating that the heterostructures exhibit superior light utilization in the visible and ultraviolet regions compared to

monolayers. This enhancement in the absorption coefficient of light is attributed to charge transfer, vacancies, and interplanar coupling. These factors collectively improve the photocatalytic performance of heterostructures for water splitting.

CONCLUSIONS

In summary, density functional theory (DFT) calculations were employed to investigate the electronic characteristics and photocatalytic mechanism of BAs/Janus-MoSeTe and BAs/Janus-MoTeSe heterostructures. The stability of these heterostructures was verified by phonon spectrum analysis. Our results revealed the formation of Type-II and Z-scheme heterostructures with direct band gap values of 1.18 eV and 0.66 eV, respectively. Introducing Se vacancies further reduced the interlayer band gap while increasing the effective mass of electrons and holes. Charge redistribution at the interface induced a built-in electric field. Upon interaction with visible light, this built-in electric field accumulated photoinjected holes in the VBM of Janus-WSeTe or Janus-WTeSe and photoinjected electrons in the CBM of BAs. Overall, the Z-scheme (BAs/Janus-WTeSe) exhibited superior catalytic efficiency compared to the Type-II (BAs/Janus-WSeTe) heterostructure, demonstrating its potential as a promising catalyst for water splitting.

AUTHOR CONTRIBUTIONS

Conceptualisation of work: HBB, AJ, SZI, AGN and DDT; **Conducting of experiments:** HBB and AGN; **Computation:** HBB and AGN; **Data analyses:** HBB, SZI, AGN and DDT; **Data dissemination & graphics:** HBB, SZI, AGN, and DDT; **Writing of manuscript:** HBB, AJ, AGN, and DDT; **Project support:** DDT.

CONFLICTS OF INTEREST

There are no conflicts to declare.

AUTHOR INFORMATION

Corresponding Author

*** Email: azeem.nabi@uog.edu.pk; imagnabi@gmail.com (AGN)**

*** Email: d.ditommaso@qmul.ac.uk (D.D.T).**

ORCID

Azeem Ghulam Nabi - orcid.org/0000-0002-3007-1235

Devis Di Tommaso - orcid.org/0000-0002-4485-4468

ACKNOWLEDGMENTS

Calculations were performed using the U.K. National Supercomputing Facility ARCHER2 (http://www.archer2.ac.uk) via our membership of the U.K.'s HEC Materials Chemistry Consortium, which is funded by the EPSRC (Grants EP/L000202 and EP/R029431) and the Molecular Modelling Hub for computational resources, MMM Hub, which is partially funded by EPSRC (EP/P020194/1). This research has also utilized Queen Mary's Apocrita HPC facility, supported by QMUL Research-IT.

REFERENCES

[1] N. Raza, W. Raza, H. Gul, and K. H. Kim, "ZnO–ZnTe hierarchical superstructures as solar-light-activated photocatalysts for azo dye removal," *Environ Res*, vol. 194, no. November 2020, p. 110499, 2021, doi: 10.1016/j.envres.2020.110499.

[2] R. M. Navarro Yerga, M. Consuelo Álvarez Galván, F. del Valle, J. A. Villoria de la Mano, and J. L. G. Fierro, "Water splitting on semiconductor catalysts under visiblelight irradiation," *ChemSusChem*, vol. 2, no. 6. Wiley-VCH Verlag, pp. 471–485, 2009. doi: 10.1002/cssc.200900018.

[3] S. Wang, C. Ren, H. Tian, J. Yu, and M. Sun, "MoS2/ZnO van der Waals heterostructure as a high-efficiency water splitting photocatalyst: A first-principles study," *Physical Chemistry Chemical Physics*, vol. 20, no. 19, pp. 13394–13399, 2018, doi: 10.1039/c8cp00808f.

[4] X. Ma, X. Wu, H. Wang, and Y. Wang, "A Janus MoSSe monolayer: A potential wide solar-spectrum water-splitting photocatalyst with a low carrier recombination rate," *J Mater Chem A Mater*, vol. 6, no. 5, pp. 2295–2301, 2018, doi: 10.1039/c7ta10015a.

[5] T. W. Kim, D. Kim, Y. Jo, J. Park, H. S. Kim, and C. H. Shin, "Van der Waals Heteroepitaxy of Te Crystallites/2H-MoTe2 Atomically Thin Films on GaAs Substrates by Using Metal-Organic Chemical-Vapor Deposition," *Journal of the Korean Physical Society*, vol. 76, no. 2, pp. 167–170, Jan. 2020, doi: 10.3938/jkps.76.167.

[6] M. Cao *et al.*, "DFT investigation on direct Z-scheme photocatalyst for overall water splitting: MoTe2/BAs van der Waals heterostructure," *Appl Surf Sci*, vol. 551, Jun. 2021, doi: 10.1016/j.apsusc.2021.149364.

[7] A. Nabi, "The electronic and the magnetic properties of Mn doped wurtzite CdS: First-principles calculations," *Comput Mater Sci*, vol. 112, pp. 210–218, Feb. 2016, doi: 10.1016/j.commatsci.2015.10.039.

[8] D. H. Lim, J. H. Jo, D. Y. Shin, J. Wilcox, H. C. Ham, and S. W. Nam, "Carbon dioxide conversion into hydrocarbon fuels on defective graphene-supported Cu nanoparticles from first principles," *Nanoscale*, vol. 6, no. 10, pp. 5087–5092, 2014, doi: 10.1039/c3nr06539a.

[9] M. Akhtar *et al.*, "Recent advances in synthesis, properties, and applications of phosphorene," *npj 2D Materials and Applications*, vol. 1, no. 1. Nature Publishing Group, Dec. 01, 2017. doi: 10.1038/s41699-017-0007-5.

[10] S. Joseph *et al.*, "A review of the synthesis, properties, and applications of 2D transition metal dichalcogenides and their heterostructures," *Mater Chem Phys*, vol. 297, Mar. 2023, doi: 10.1016/j.matchemphys.2023.127332.

[11] Y. Gogotsi and Q. Huang, "MXenes: Two-Dimensional Building Blocks for Future Materials and Devices," *ACS Nano*, vol. 15, no. 4. American Chemical Society, pp. 5775–5780, Apr. 27, 2021. doi: 10.1021/acsnano.1c03161.

[12] Y. Guan, X. Li, Q. Hu, D. Zhao, and L. Zhang, "Theoretical design of BAs/WX2 (X = S, Se) heterostructures for high-performance photovoltaic applications from DFT calculations," *Appl Surf Sci*, vol. 599, Oct. 2022, doi: 10.1016/j.apsusc.2022.153865.

[13] A. Y. Lu *et al.*, "Janus monolayers of transition metal dichalcogenides," *Nat Nanotechnol*, vol. 12, no. 8, pp. 744–749, Aug. 2017, doi: 10.1038/nnano.2017.100.

[14] A. Singh, M. Jain, and S. Bhattacharya, "MoS2and Janus (MoSSe) based 2D van der Waals heterostructures: Emerging direct Z-scheme photocatalysts," *Nanoscale Adv*, vol. 3, no. 10, pp. 2837–2845, May 2021, doi: 10.1039/d1na00154j.

[15] Z. Guan, S. Ni, and S. Hu, "Tunable Electronic and Optical Properties of Monolayer and Multilayer Janus MoSSe as a Photocatalyst for Solar Water Splitting: A First-Principles Study," *Journal of Physical Chemistry C*, vol. 122, no. 11, pp. 6209–6216, Mar. 2018, doi: 10.1021/acs.jpcc.8b00257.

[16] Z. Chen, H. Liu, X. Chen, G. Chu, S. Chu, and H. Zhang, "Wafer-Size and Single-Crystal MoSe2 Atomically Thin Films Grown on GaN Substrate for Light Emission and Harvesting," *ACS Appl Mater Interfaces*, vol. 8, no. 31, pp. 20267–20273, Aug. 2016, doi: 10.1021/acsami.6b04768.

[17] S. K. Jain *et al.*, "2D/3D Hybrid of MoS2/GaN for a High-Performance Broadband Photodetector," *ACS Appl Electron Mater*, vol. 3, no. 5, pp. 2407–2414, May 2021, doi: 10.1021/acsaelm.1c00299.

[18] A. Albar and S. A. Aravindh, "Emergence of metallic states at 2D MoSSe/GaAs Janus interface: A DFT study," *Journal of Physics Condensed Matter*, vol. 33, no. 47, Nov. 2021, doi: 10.1088/1361-648X/ac2202.

[19] M. Moun, M. Kumar, M. Garg, R. Pathak, and R. Singh, "Understanding of MoS2/GaN Heterojunction Diode and its Photodetection Properties," *Sci Rep*, vol. 8, no. 1, Dec. 2018, doi: 10.1038/s41598-018-30237-8.

[20] Z. Zhang, Q. Qian, B. Li, and K. J. Chen, "Interface Engineering of Monolayer MoS2/GaN Hybrid Heterostructure: Modified Band Alignment for Photocatalytic Water Splitting Application by Nitridation Treatment," *ACS Appl Mater Interfaces*, vol. 10, no. 20, pp. 17419–17426, May 2018, doi: 10.1021/acsami.8b01286.

[21] D. Xu, B. Zhai, Q. Gao, T. Wang, J. Li, and C. Xia, "Interface-controlled band alignment transition and optical properties of Janus MoSSe/GaN vdW heterobilayers," *J Phys D Appl Phys*, vol. 53, no. 5, 2020, doi: 10.1088/1361-6463/ab50f9.

[22] K. Manoharan and V. Subramanian, "Exploring Multifunctional Applications of Hexagonal Boron Arsenide Sheet: A DFT Study," *ACS Omega*, vol. 3, no. 8, pp. 9533–9543, Aug. 2018, doi: 10.1021/acsomega.8b00946.

[23] S. Han, Y. Li, and Z. Wang, "AlAs/SiH van der Waals heterostructures: A promising photocatalyst for water splitting," *Physica E Low Dimens Syst Nanostruct*, vol. 134, p. 114869, Oct. 2021, doi: 10.1016/j.physe.2021.114869.

[24] A. Ohtake and Y. Sakuma, "Effect of Substrate Orientation on MoSe2/GaAs Heteroepitaxy," *Journal of Physical Chemistry C*, 2020, doi: 10.1021/acs.jpcc.9b11278.

[25] F. Wen, J. Yuan, K. S. Wickramasinghe, W. Mayer, J. Shabani, and E. Tutuc, "Epitaxial Al-InAs Heterostructures as Platform for Josephson Junction Field-Effect Transistor Logic Devices," *IEEE Trans Electron Devices*, vol. 68, no. 4, pp. 1524–1529, Apr. 2021, doi: 10.1109/TED.2021.3057790.

[26] M. Xu, J. Yang, C. Sun, L. Liu, Y. Cui, and B. Liang, "Performance enhancement strategies of bi-based photocatalysts: A review on recent progress," *Chemical Engineering Journal*, vol. 389. Elsevier B.V., Jun. 01, 2020. doi: 10.1016/j.cej.2020.124402.

[27] J. Heyd, G. E. Scuseria, and M. Ernzerhof, "Hybrid functionals based on a screened Coulomb potential," *Journal of Chemical Physics*, vol. 118, no. 18, pp. 8207–8215, May 2003, doi: 10.1063/1.1564060.

[28] G. Z. Wang, S. H. Dang, W. X. Zhao, Y. D. Li, S. Y. Xiao, and M. M. Zhong, "Tunable Photocatalytic Properties of GaN-Based Two-Dimensional Heterostructures," *Phys Status Solidi B Basic Res*, vol. 255, no. 8, Aug. 2018, doi: 10.1002/pssb.201800133.

[29] C. Chen *et al.*, "Ambient-Stable Black Phosphorus-Based 2D/2D S-Scheme Heterojunction for Efficient Photocatalytic CO2Reduction to Syngas," *ACS Appl Mater Interfaces*, vol. 13, no. 17, pp. 20162–20173, 2021, doi: 10.1021/acsami.1c03482.

[30] N. Su, Z. Zhang, P. Fay, H. P. Moyer, R. D. Rajavel, and J. Schulman, "V© World Scientific TEMPERATURE-DEPENDENT MICROWAVE PERFORMANCE OF SB-HETEROSTRUCTURE BACKWARD DIODES FOR MILLIMETER-WAVE DETECTION," 2007. [Online]. Available: www.worldscientific.com

[31] Z. Yang and J. Hao, "Recent Progress in 2D Layered III–VI Semiconductors and their Heterostructures for Optoelectronic Device Applications," *Advanced Materials Technologies*, vol. 4, no. 8. Wiley-Blackwell, Aug. 01, 2019. doi: 10.1002/admt.201900108.

[32] C. C. Liu, W. Feng, and Y. Yao, "Quantum spin Hall effect in silicene and two-dimensional germanium," *Phys Rev Lett*, vol. 107, no. 7, Aug. 2011, doi: 10.1103/PhysRevLett.107.076802.

[33] S. Kar, P. Kumari, M. V. Kamalakar, and S. J. Ray, "Twist-assisted optoelectronic phase control in two-dimensional (2D) Janus heterostructures," *Sci Rep*, vol. 13, no. 1, Dec. 2023, doi: 10.1038/s41598-023-39993-8.

[34] A. Abid, M. Haneef, S. Ali, and A. Dahshan, "A study of 2H and 1T phases of Janus monolayers and their van der Waals heterostructure with black phosphorene for optoelectronic and thermoelectric applications," *J Solid State Chem*, vol. 311, Jul. 2022, doi: 10.1016/j.jssc.2022.123159.

[35] W. Yang *et al.*, "III-V compound materials and lasers on silicon," *Journal of Semiconductors*, vol. 40, no. 10. Institute of Physics Publishing, 2019. doi: 10.1088/1674-4926/40/10/101305.

[36] L. V. Begunovich *et al.*, "Triple VTe2/graphene/VTe2 heterostructures as perspective magnetic tunnel junctions," *Appl Surf Sci*, vol. 510, Apr. 2020, doi: 10.1016/j.apsusc.2020.145315.

[37] Y. Guan, X. Li, Q. Hu, D. Zhao, and L. Zhang, "Theoretical design of BAs/WX2 (X = S, Se) heterostructures for high-performance photovoltaic applications from DFT calculations," *Appl Surf Sci*, vol. 599, Oct. 2022, doi: 10.1016/j.apsusc.2022.153865.

[38] H. Ye, H. Sheng, D. Bai, J. Zhang, and J. Wang, "Strain and electric field tuned electronic properties of BAs/MoSe2 van der Waals heterostructures for alternative electrodes and photovoltaic cell in photocatalysis," *Physica E Low Dimens Syst Nanostruct*, vol. 120, Jun. 2020, doi: 10.1016/j.physe.2020.114055.

[39] R. Q. Sheng, X. Q. Deng, Z. H. Zhang, and Z. Q. Fan, "Tunable electronic and optical properties of SnC/BAs heterostructure by external electric field and vertical strain," *Physics Letters, Section A: General, Atomic and Solid State Physics*, vol. 384, no. 7, Mar. 2020, doi: 10.1016/j.physleta.2019.126150.

[40] L. Jiankang, L. Cheng, L. Jie, J. Bing, J. Zhenyi, and H. Sheng, "Design of GaN/Janus-WSSe vdW heterostructure for photocatalytic water splitting: ab initio calculations," *Journal of the Korean Physical Society*, vol. 82, no. 12, pp. 1180–1186, Jun. 2023, doi: 10.1007/s40042-023-00782-1.

[41] G. Kresse and D. Joubert, "From ultrasoft pseudopotentials to the projector augmented-wave method," *Phys Rev B*, vol. 59, no. 3, p. 1758, 1999.

[42] P. E. Blöchl, "Projector augmented-wave method," *Phys Rev B*, vol. 50, no. 24, p. 17953, 1994.

[43] J. P. Perdew, K. Burke, and M. Ernzerhof, "Generalized gradient approximation made simple," *Phys Rev Lett*, vol. 77, no. 18, p. 3865, 1996.

[44] S. Grimme, J. Antony, S. Ehrlich, and H. Krieg, "A consistent and accurate ab initio parametrization of density functional dispersion correction (DFT-D) for the 94 elements H-Pu," *J Chem Phys*, vol. 132, no. 15, p. 154104, 2010.

[45] J. Heyd, G. E. Scuseria, and M. Ernzerhof, "Hybrid functionals based on a screened Coulomb potential," *J Chem Phys*, vol. 118, no. 18, pp. 8207–8215, 2003.

[46] R. Iftimie, P. Minary, and M. E. Tuckerman, "Ab initio molecular dynamics: Concepts, recent developments, and future trends," 2005. [Online]. Available: www.pnas.orgcgidoi10.1073pnas.0500193102

[47] I. Ahmad, I. Shahid, A. Ali, S. Zeb, L. Gao, and J. Cai, "The van der Waals CdO/PtS2heterostructures for photocatalytic water splitting with excellent carrier separation and light absorption," *New Journal of Chemistry*, vol. 45, no. 37, pp. 17699–17708, Oct. 2021, doi: 10.1039/d1nj03232a.

[48] P. G. Risueño, P. Han, and G. Bester, "Frozen-phonon method for state anticrossing situations and its application to zero-point motion effects in diamondoids."

[49] Z. Zhou, X. Niu, Y. Zhang, and J. Wang, "Janus MoSSe/WSeTe heterostructures: A direct Z-scheme photocatalyst for hydrogen evolution," *J Mater Chem A Mater*, vol. 7, no. 38, pp. 21835–21842, 2019, doi: 10.1039/c9ta06407a.

[50] Y. Sun, Z. Shuai, and D. Wang, "Janus monolayer of WSeTe, a new structural phase transition material driven by electrostatic gating," *Nanoscale*, vol. 10, no. 46, pp. 21629–21633, Dec. 2018, doi: 10.1039/c8nr08151d.

[51] M. Kepenekian *et al.*, "Concept of Lattice Mismatch and Emergence of Surface States in Two-dimensional Hybrid Perovskite Quantum Wells," *Nano Lett*, vol. 18, no. 9, pp. 5603–5609, Sep. 2018, doi: 10.1021/acs.nanolett.8b02078.

[52] T. N. Do *et al.*, "Type-I band alignment of BX-ZnO (X = As, P) van der Waals heterostructures as high-efficiency water splitting photocatalysts: a first-principles study," *RSC Adv*, vol. 10, no. 72, pp. 44545–44550, Nov. 2020, doi: 10.1039/d0ra09701b.

[53] J. Hermann, R. A. DiStasio, and A. Tkatchenko, "First-Principles Models for van der Waals Interactions in Molecules and Materials: Concepts, Theory, and Applications," *Chemical Reviews*, vol. 117, no. 6. American Chemical Society, pp. 4714–4758, Mar. 22, 2017. doi: 10.1021/acs.chemrev.6b00446.

[54] R. Zhang *et al.*, "A black Phosphorus/BiVO4(010) heterostructure for promising photocatalytic performance: First-principles study," *Journal of Physics and Chemistry of Solids*, vol. 143, Aug. 2020, doi: 10.1016/j.jpcs.2020.109466.

[55] G. Zhang, Z. Wang, and J. Wu, "Construction of a Z-scheme heterojunction for high-efficiency visible-light-driven photocatalytic CO2reduction," *Nanoscale*, vol. 13, no. 8. Royal Society of Chemistry, pp. 4359–4389, Feb. 28, 2021. doi: 10.1039/d0nr08442e.

[56] Z. Zhou, X. Niu, Y. Zhang, and J. Wang, "Janus MoSSe/WSeTe heterostructures: A direct Z-scheme photocatalyst for hydrogen evolution," *J Mater Chem A Mater*, vol. 7, no. 38, pp. 21835–21842, 2019, doi: 10.1039/c9ta06407a.